Chapter 6

GEOMORPHIC CONTROLS OF LANDSAT BASED THERMAL PATTERNS

6.1 Introduction

River temperature is the key parameter in aquatic ecosystems as it influences habitat conditions. (Caissie, 2006; Ling et al., 2017; Smith, 2008; Wawrzyniak et al., 2012). Several water quality parameters like dissolved oxygen (DO), pH, salinity, and suspended sediment concentration depend upon river water temperature (Terzi and Verep, 2011; Viswanathan et al., 2015). The increase of river temperature above a certain threshold can decrease aquatic life or increase stress, even death of some species (Eaton et al., 1995; Mohseni et al., 2003; Xin and Kinouchi 2013).

The thermal patterns of a river are generally affected by the local climate, river morphology, anthropogenic activities, and geographical setting (Caissie, 2006). The type of river can also greatly influence the flow temperature; for example, river temperature in braided streams is highly heterogeneous due to their habitat diversity, channel complexity, and the presence of groundwater inputs (Mosley,1983; Wawrzyniak et al., 2016). As greater attention is being paid to global warming these days, the research into spatial and thermal patterns of the river is essential for fluvial science and management. The primary purpose of water resource management is to ameliorate the hydrologic extremes to ensure public health and safety and to

relocate and redistribute available water for various uses (Clark et al., 2001; Flebbe et al., 2006; Mohseni et al., 2003).

River temperature surveys are usually based on field sensors. More recently, remote sensing technology, such as drones, UAVs (Unmanned Aerial Veichels), and satellite images, has also been used for river temperature surveys (Gholizadeh et al.,2016). Remote sensing techniques can monitor and identify large-scale regions and water bodies that suffer from qualitative problems more effectively and efficiently(Kondratyev et al., 1998; Hadjimitsis and Clayton, 2009). The output from remotely sensed instruments comes in digital form so that it can be very quickly processed in computer systems (Koponen et al., 2002). Remote sensing-based techniques have been widely used for river temperature sampling in the contemporary world (Ritchie et al., 2003). Information sharing through the internet reduces data acquisition time and thus provides an efficient way to carry out real-time thermal estimation. Involving remote sensing with GIS makes it a potent tool to identify the indicators of thermal patterns in the riverine ecosystem.

Satellite TIR (thermal Infra-red) can also be applicable to large rivers (Handcock et al., 2006; Lalot et al., 2015). Satellite thermal data, which are available in the public domain, consisting of Landsat series data (Landsat-5, Landsat-7, Landsat-8) and MODIS data. Thermal resolution for Landsat-5, Landsat-7, and Landsat-8 are 120 meters, 60 meters, and 100 meters. For ASTER data, the thermal resolution is 90 meters. Only thermal patterns of large rivers can be made with satellite images because the resolution is still coarse. The channel width must be more than three pixels to be meaningful, decrease the effect of near-bank reflected radiance, and calculate consistent water surface temperatures. So, according to the three pixels width requirement, temperature mapping can be done for those rivers whose widths are wider than

180m to 360m (Wawrzyniak et al., 2012; Cardona et al.,2019). The Landsat 8 Operational Land Imager (OLI) and Thermal Infrared Sensor (TIRS) is the 8th satellite in the Landsat program. It has two thermal infrared bands at about 10.9 and 12μm with a spatial resolution of 100 meters. Landsat 8 thermal band has a lower spatial resolution in comparison to 60 meters of Landsat 7 Enhanced Thematic Mapper Plus (ETM+). However, the two thermal bands of Landsat 8 are highly effective in thermal image examination capacity in contrast to the past single-channel imagers. Also, the data gap due to scan line corrector malfunction has limited the usability of Landsat 7 images since 2003 (Reuter et al.,2015; Wawrzyniak et al., 2012).

The Landsat satellite provides continuous periodic coverage over a large area and is also freely accessible. Their archives permit the assemblage of a large number of images to address seasonal and inter-annual variability. Unlike airborne imagery, satellite images can be used for large continuous thermal profiles over hundreds of kilometers when a thermal sensor is deployed. An airborne sensor takes several days to fly over a large river stretch, and there can be discrepancies between successive flights. Moreover, it is very costly to survey the study stretch using airborne flights for a continuous period. Further, due to the cost of overflights, the temporal coverage achievable with airborne remote sensing is also limited, and, in most studies, only a few thermal images are acquired over time (Handcock et al., 2006; Wawrzyniak et al., 2012). Fluvial research dependent on the Landsat program is broad; however, water temperature analysis got little attention (Baban, 1993; Frazier and Page, 2000; Kay et al., 2005).

Some scientists have found that surface water temperature is generally close to the groundwater temperature at the source and increases after that with distance/stream order. The water temperature increase does not follow a linear pattern. Besides, the temperature increase rate is

more significant for smaller streams than for larger streams. The rate for smaller streams has been recorded as 0.6°C $km^{-1,}$ and for larger streams, that have been 0.09°C km^{-1}(Zwieniecki and Newton, 1999; Torgersen et al., 2001). Small scale variation of the thermal patterns of the river can be observed downstream of the confluence (Ebersole et al., 2003) in seepage areas in pools (Matthews et al., 1994) and at microhabitat scales (Clark et al., 1999). The type of river also affects the thermal pattern. The braided rivers can experience inflated water temperature because the small and shallow channels are highly exposed to meteorological conditions (Mosley 1983). Anthropogenic activities and climate change also increase river temperature (Steel et al., 2017; Fullerton et al., 2018). The construction of dams and thermal or nuclear power plants nearby rivers can also affect the river's thermal heterogeneity spatially and temporally (Wawrzyniak et al., 2012; Ling et al., 2017; Mejia et al.,2020).

River morphology affects the longitudinal pattern of river temperature, which includes in-stream morphological features like pools and riffles and off-stream morphological features like sandbars, point bars, alluvial plain, river island, and, channel shifting, etc. (Winfree et al., 2018). Among the different parameters used in geomorphology, the Sinuosity index can be used to assess changes in the overall course of a river. According to Jerry E. Mueller, “Stream sinuosity indexes are usually derived by dividing the length of a reach as measured along a channel by the length of a reach as measured along a valley” (Mueller, 1968). Several other indices exist, such as the Wolman index or Brice index. However, most indexes show limits in their measurement feasibility, applicability, and universal acceptance (Eziashi, 1999; Ghosh and Mistri, 2012). With the increasing quality, acquisition frequency, and availability of satellite images, planform metrics of large rivers can now be easily measured and assessed. Sensors of the satellite can catch the radiation energy of the different earth features not only in

the visible region of the electromagnetic (EM) spectrum but can also capture radiation energy over an expansive range of EM spectrums. It can provide additional information, which otherwise is difficult to measure (Dash et al., 2002; Lamaro et al., 2013).

In this chapter, thermal analysis has been performed for the river Ganga, a huge and wide river (approximate width through the entire study stretch is 700 meters) characterized by a sand-bed wandering channel. This contribution aims (1) to detect thermal patterns over a reach of 240 km at fairly low flow (2) to explore seasonal and interannual variability.

Figure 6.1 shows the entire stretch's location, the satellite scenes id’s over the region, and the Central water commission (CWC) station.

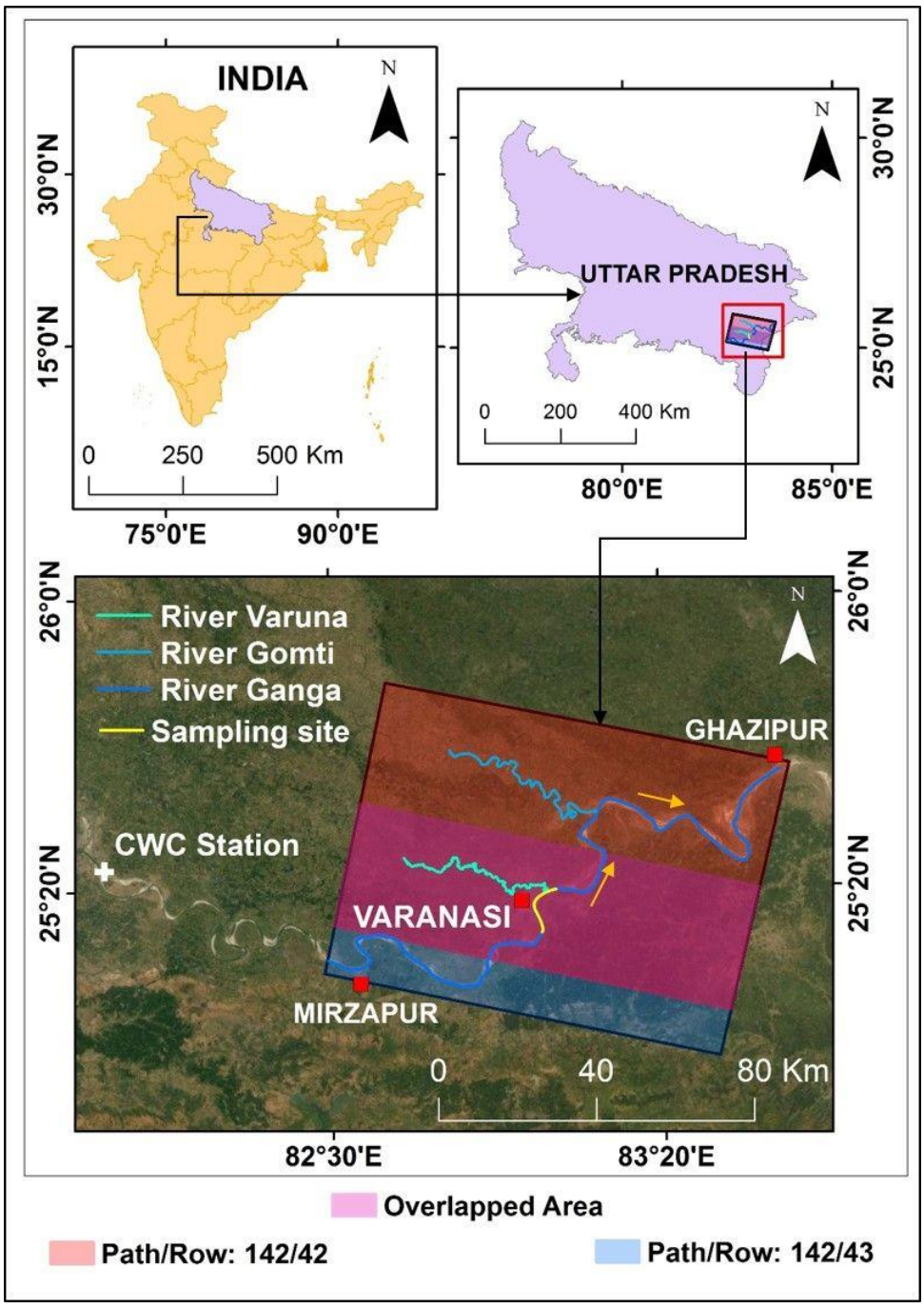

Figure 6.1 Location map showing the study region

6.2 Data

Two Landsat scenes were selected for the study, and those scenes have path id "142" and row id "42" and "43". Eight images have been downloaded for this work. A series of cloud-free images for the months of February and June (mostly) for each year under consideration has been downloaded (Table 1). The software used for processing Landsat-8 datasets has been Google Earth Engine (GEE) and ArcGIS 10.5.

Table 6.1 Date of acquisition of the median air temperature values for the whole study stretch and River stage at Prayagraj Hydrological station (CWC station) along with velocity values

Satellite Acquisition dates	Air temperature (°C)	River stage at Prayagraj Hydrological Station (m.a.s.l)	Water temperature (°C)	Velocity value (m/s) Wide section	Velocity value (m/s) Narrow section
13-Feb-14	15.6	73.31	15.86		
16-Feb-15	16.4	72.13	17.47	0.41	0.63
19-Feb-16	17.5	71.52	21.68	0.42	0.63
21-Feb-17	16.7	71.81	20.49	0.39	0.58
24-Feb-18	17.1	72.09	21.63		
05-Jun-14	28.8	70.8	30.60		
08-Jun-15	29.9	71.85	27.62	0.54	0.74
10-Jun-16	29.8	71.19	24.41	0.53	0.72
13-Jun-17	30.7	71.53	27.31	0.54	0.69
15-May-18	24.6	71.89	23.60		

6.3 Materials and methods

Apart from river temperature estimation, work consists of several steps like image classification, river feature layer extraction, river shapefile creation, centerline vectorization, sinuosity calculation, active width and wetted width determination, river temperature calculation, mixed pixel exclusion, and lastly, the analysis of the seasonal and interannual variability of the river thermal pattern

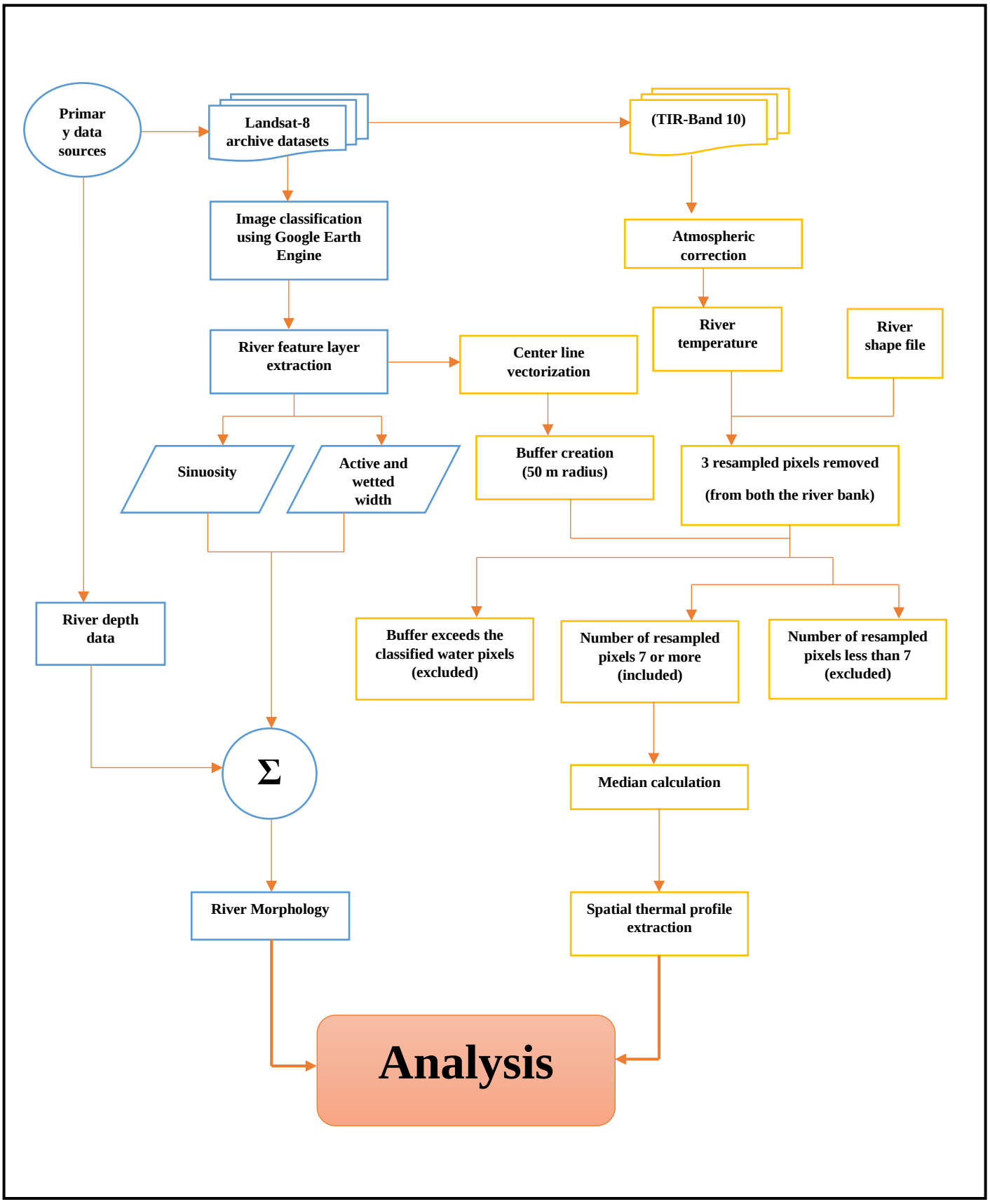

Figure 6.2 Flowchart of the methodology adopted for the work

6.3.1 Extraction of flow channel and sandbars from Image Classification

Google Earth Engine (GEE) facilitates a fast analysis platform by using Google's computing infrastructure. GEE provides online access to archived Landsat data as a collection of the USGS (Huang et al., 2017). Pre-processed Landsat imagery available through GEE was used to assess the river and sandbars across the study area.

One of the supervised classification techniques, known as Classification and Regression Trees (CART) was used for classifying the imagery into two classes, namely Water and Sandbars. This classification has been done in the GEE platform.

Table 6.2 OA and kappa values of the Classification and Regression Trees for water and sand bars pixels of the eight studied dates

Satellite acquisition dates	User's accuracy %		Producer's accuracy %		Overall accuracy (OA) %	Kappa (κ) coefficient
	Water	Sandbars	Water	Sandbars		
16 February 2015	86.74	84.63	94.67	94.64	90.71	0.88
19 February 2016	86.25	84.24	94.38	94.29	89.32	0.85
21 February 2017	86.57	84.78	94.43	94.36	89.37	0.86
24 February 2018	82.23	80.34	93.27	93.21	87.84	0.84
8 June 2015	82.19	80.11	93.82	93.78	88.53	0.85
10 June 2016	81.89	80.02	93.12	93.06	87.24	0.84
13 June 2017	86.75	85.88	94.69	94.65	90.74	0.85
15 May 2018	88.42	86.34	94.87	94.83	91.63	0.87
Average	85.13	83.31	94.15	94.10	89.42	0.85
Std. Dev*	2.35	4.37	3.76	5.46	3.25	0.1

*Std. Dev is Standard Deviation

The water class has better User's and Producer's accuracy as compared to the sandbar class. The standard deviation value has also been less for the water class in comparison to the sandbar class. The process of temperature calculation from the LANDSAT-8 image has been described in Chapter 3.

6.3.2 Removal of the mixed pixels and Temperature profile extraction

The original spatial resolution of the TIRS band is 100m which USGS itself resamples to 30m. Currently, USGS doesn't give the inherent resolution data, so it is not possible to ascertain the relative position between original and resampled TIRS pixels (Cardona et al., 2019). This leads to a mixed pixel effect in new pixels. To remove the mixed pixel effect, the flow channel shapefile was extracted from the classified image and then clipped by a distance of 90m, i.e., 3 pixels from each side (Figure 6.3).

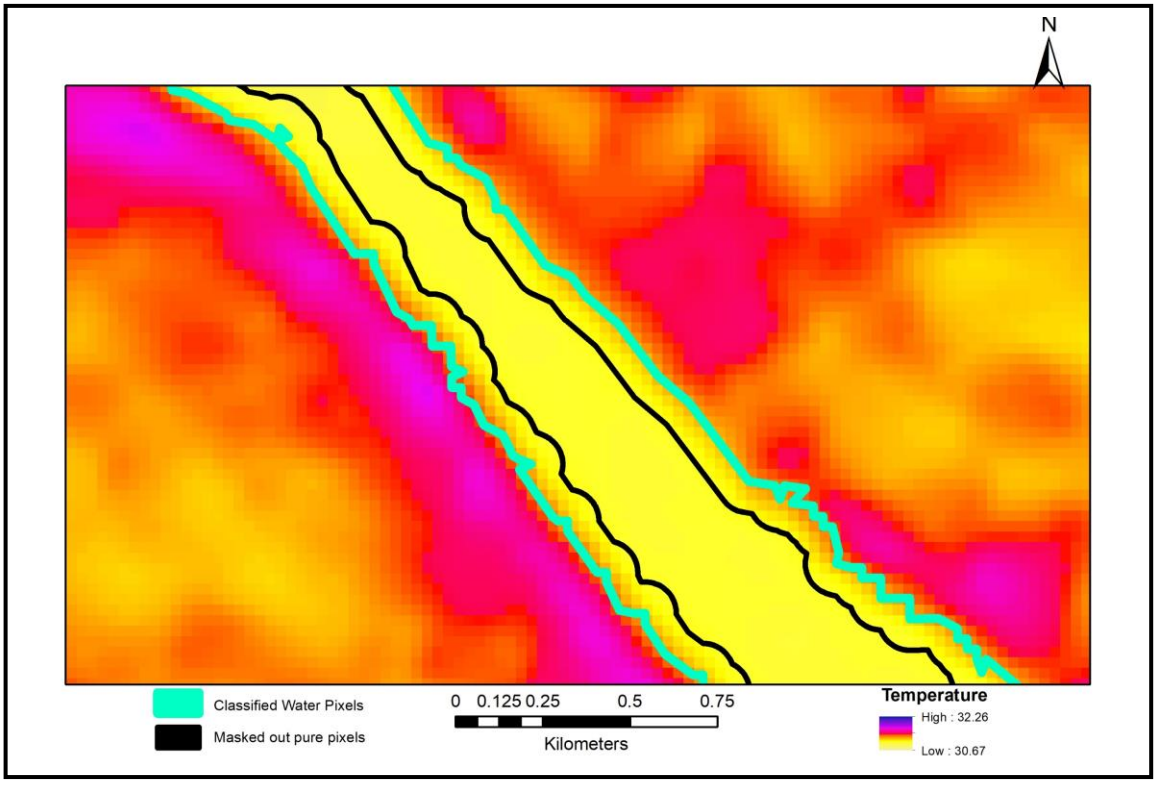

Figure 6.3 Extraction of pure water pixels

The temperature profile was extracted for each date along a centerline. Initially, the centerline was broken into points at a distance of 100m each, and then a circular buffer of 50m was created around these points. The median temperature value for each buffer was extracted from the surface temperature raster.

For the centerline creation, the fluvial corridor toolbox of ArcGIS has been used (Roux et al., 2015). This tool detects the extremities points of both the given stream network polyline and the river polygon. It uses the Thiessen polygonization over the set of obtained points to calculate the centerline. As the course of the river changes with time gradually, the centerline will also shift by a little margin. The centerline was created for each image, and the one which coincides predominantly with each centerline was taken into account. This has been done to get temperature values over the same coordinates for the same number of points.

For the exclusion of the water pixels, two scenarios have been considered. When the buffer circumference exceeds the classified pixels, it is highly possible that the buffer may get placed over the sand bar, and an anomaly in the river temperature value can occur. The second scenario for exclusion has occurred when the number of resampled pure water pixels is less than 7. The median was selected to prevent the data from different outliers. At least 3 pixels are required for median analysis. 7 to 9 resampled pixels (30 m) is equivalent to 3 original TIR pixels (100m) (Figure 6.4). Scenario B is the pure water pixel inclusion scenario. Scenarios A and C are the rejection scenarios.

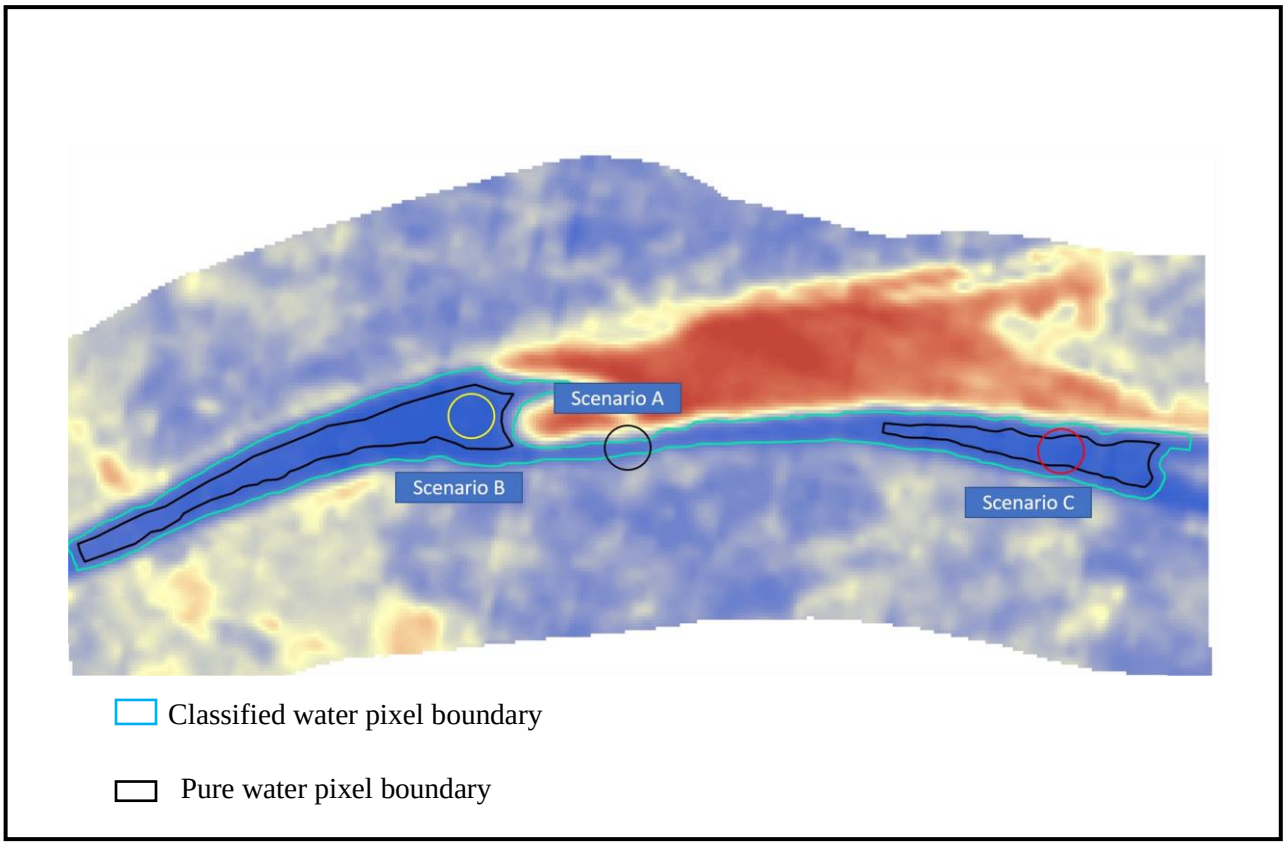

Figure 6.4 Pure water pixel inclusion and rejection scenarios for a small stretch of the study area

6.3.3 Field thermal measures for validating thermal imagery

The portable thermal sensor has been used for the field (in-situ measurement). The description of the thermal sensor has been given in Chapter 4. To validate the estimated temperatures calculated from satellite images, the results were compared with in-situ water temperatures. For this purpose, three images were selected whose acquisition dates are 25th December 2018, 10th January 2019, 11th February 2019, respectively. Since the satellite overpass through the study area was known beforehand, from the Landsat overpass calendar issued by USGS along with the approximate overpass time, the in-situ data were recorded for several points in the study area (20 for each survey) on the day of each overpass. Sixty sample points were acquired

along the mid-section of river Ganga, for which in-situ temperature was measured, and a good correlation along with RMSE value of 1.23 was observed (Figure 6.5). To mark the coordinates of the points, “Garmin Etrex 30” GPS system was used.

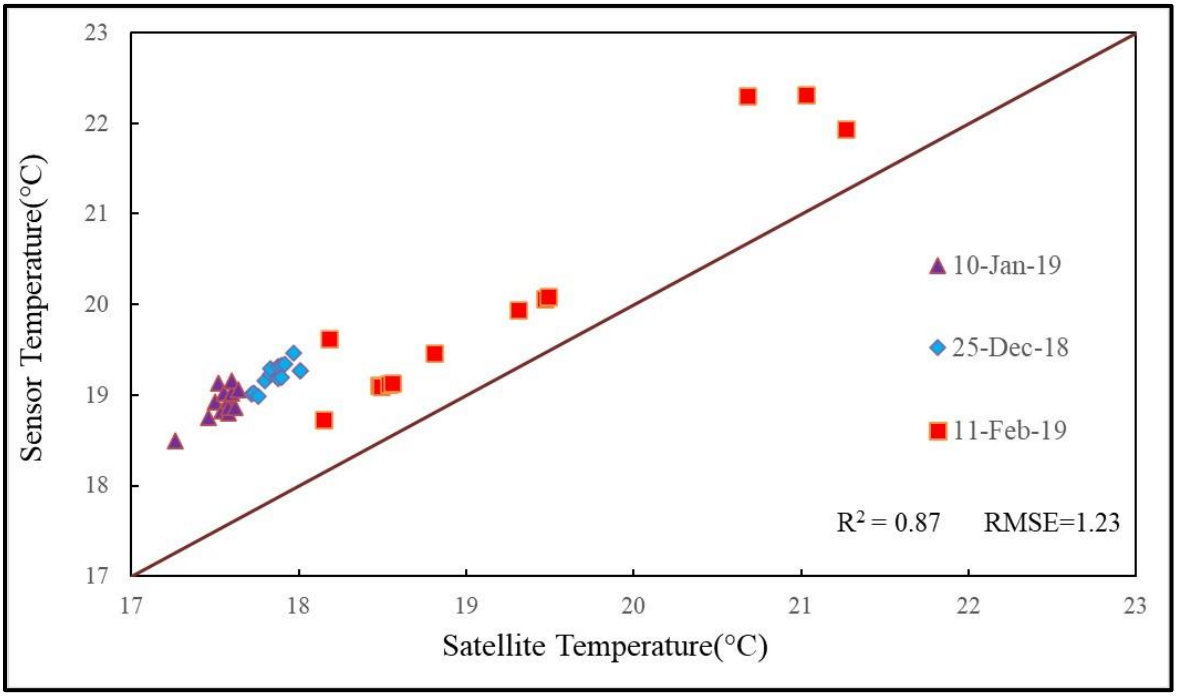

Figure 6.5 Scatterplot linking observed water temperature and LANDSAT image water temperature

The in-situ measurement has been done for the Varanasi and the nearby stretch for each sampling date. The river temperature for the month of February has been higher as compared to December and January. For each sampling date, 20 in-situ points have been measured. It has been plotted on the map and shown in figures 6.6, 6.7, and 6.8.

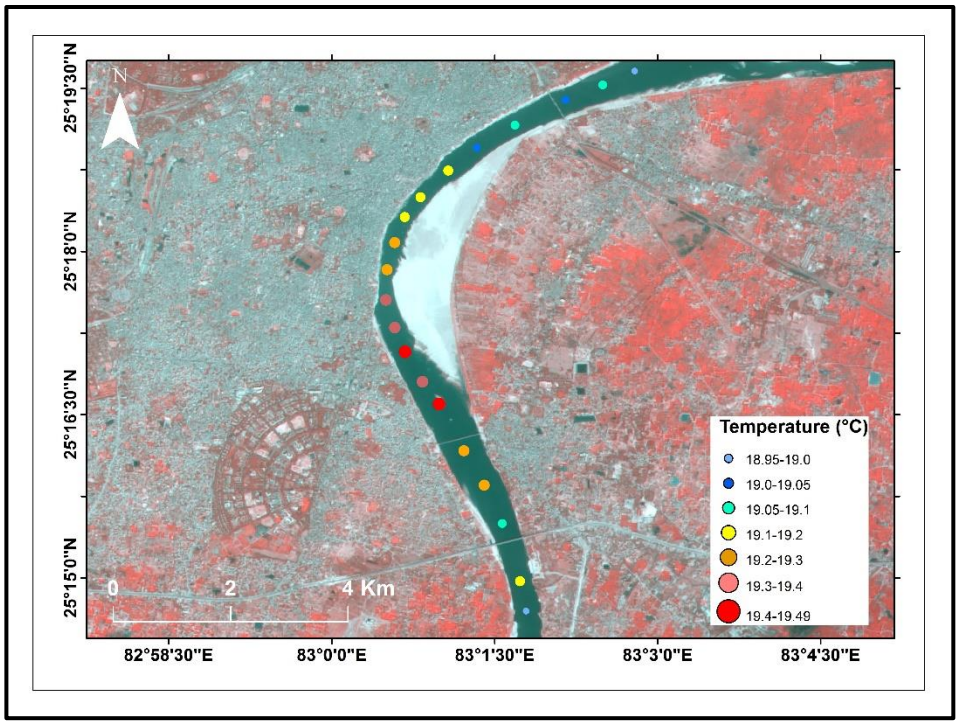

Figure 6.6 Field sampling values for 25th December 2018

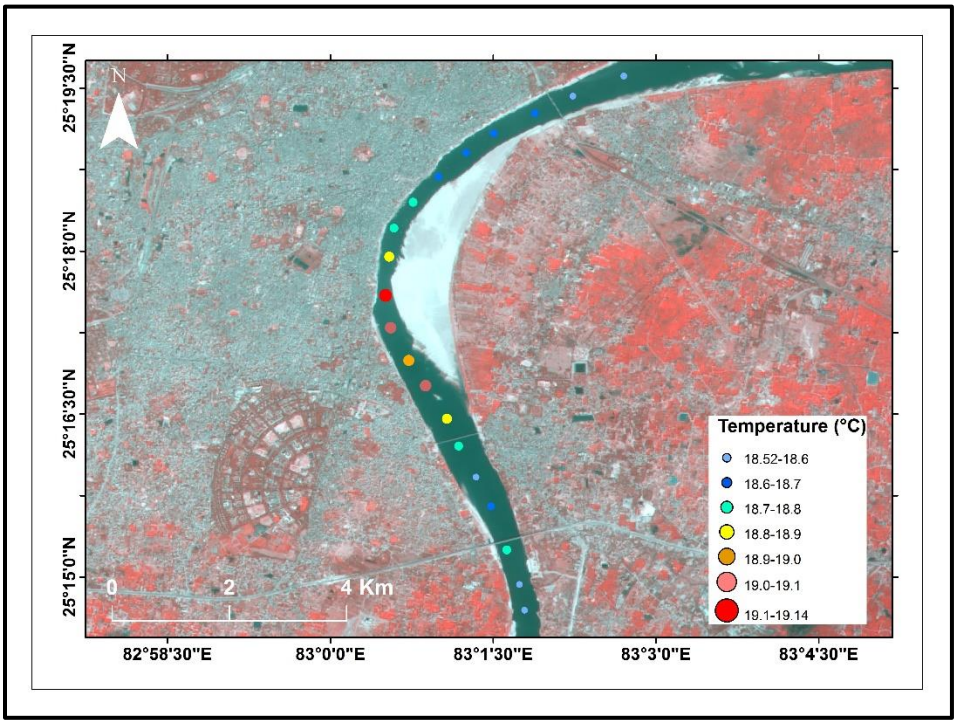

Figure 6.7 Field sampling values for 10th January 2019

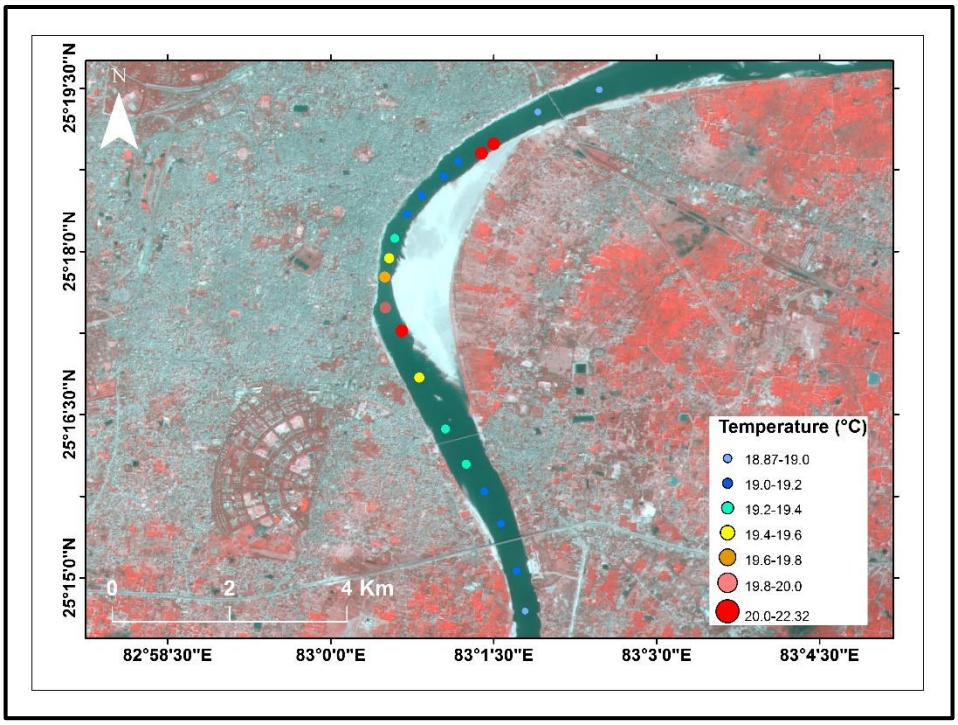

Figure 6.8 Field sampling values for 11th February 2019

6.3.4 Additional variables

6.3.4.1 Air temperature

ERA 5 datasets have been used in this analysis for the calculation of the air temperature over the entire study stretch. These datasets provide the daily climate data of the earth from 1979 in the form of gridded datasets, and the dimension of each grid is 0.25° ×0.25° (roughly 25×25 km^2). These datasets have been produced by C3S (Das et al., 2021). ERA5 band used in this analysis was 'mean_2m_air_temperature,' which records the daily average air temperature of a 0.25° ×0.25° grid at 2m height. There are 17 pixels of ERA 5 for the entire study stretch. The median air temperature value for each satellite acquisition date has been calculated for the whole study stretch (Table 6.1).

6.3.4.2 River stage and river water velocity

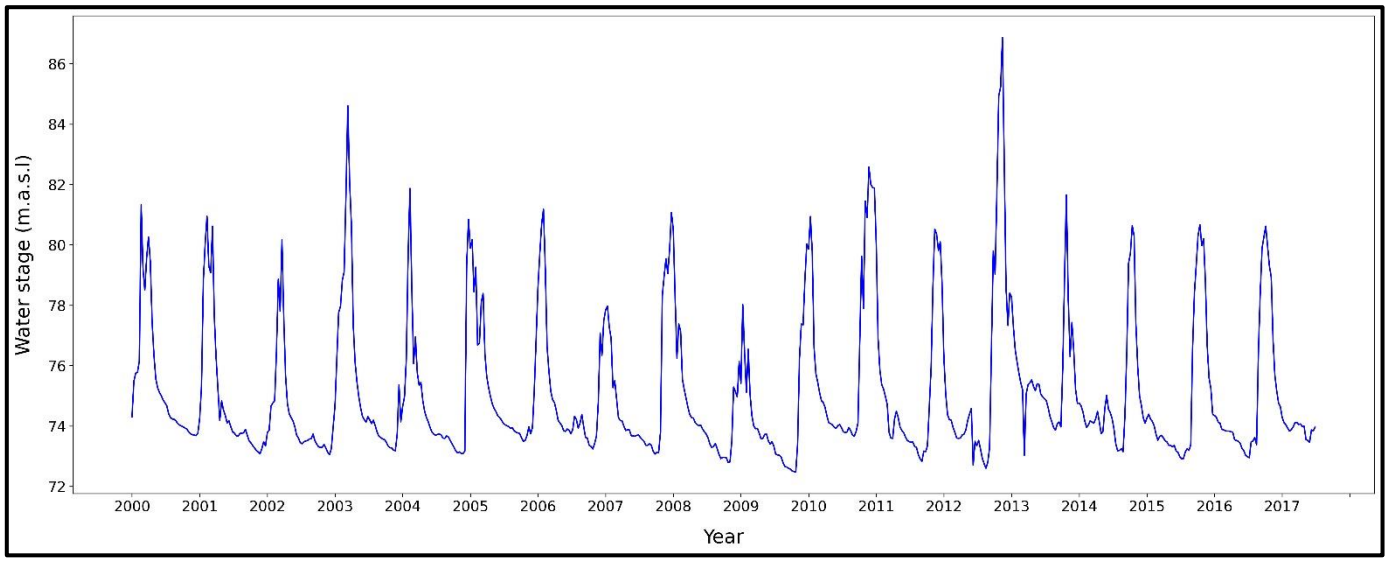

Figure 6.9 River stage value (obtained from Prayagraj CWC station)

The river stage value has been plotted for river Ganga which has been acquired from the Prayagraj CWC station. This data gives an indication of the river water level. The river velocity has been calculated by using the Manning velocity (Yu and Lim, 2003).

$$V = \frac{1}{n}\left(\sqrt[3]{(R_b)^2}\right)\left(\sqrt{S}\right) \tag{6.1}$$

where V is the depth-averaged velocity, n is the Manning's roughness coefficient, S is the channel slope, and R_b is the hydraulic radius. The value of n has been considered as 0.025 (Maddamsetty et al. 2010) for this study. The river depth data has been acquired from the National waterway authority of India (NWAI).

The river stage and the river velocity values have been tabulated in Table 6.1 for the dates under consideration.

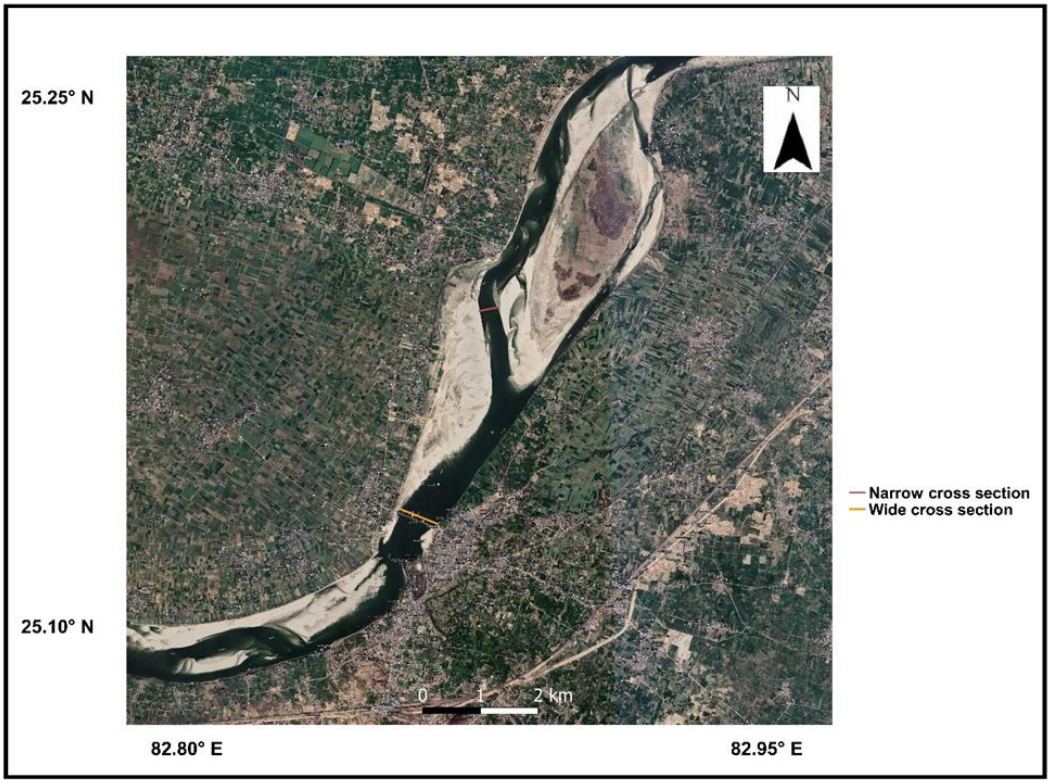

Figure 6.10 Narrow and wide cross section chosen within the study reach for measuring river velocity

6.3.4.3 River width

In this work, two types of river width have been calculated. The first one is full bank width and the second is wetted width. Wetted width (WW) corresponds to the surface channel width, which is generally wet, i.e., where water is present at the time of measurement. Bank full width is the river's cross-sectional lateral extent, which means the maximum width river can sustain without flood inundation. This is also known as active width (AW). The width was computed at each cross-section for which the temperature was calculated with the help of the width calculation tool from the Fluvial Corridor toolbox (Raux et al. 2015). The width toolbox

employs Thiessen polygons to calculate the width. It utilizes the centerline of the river to split it at defined distances and create Thiessen polygons at the center of splitted lines. Then, the width is calculated by intersecting the Thiessen polygons with the river channel polygon and connecting it to lines.

6.3.4.4 River Sinuosity index

The sinuosity index has been calculated with the help of Landsat-8 satellite images for different years in the study stretch. Muller sinuosity index has been used (Muller 1968; Ghosh and Saha 2019).

$$\text{Sinuosity index (SI)} = AL/SL \tag{6.2}$$

where AL is the actual length and SL is the straight length of the river region for which SI has been measured. The entire study reach has been divided into twenty straight lines, each having a length of 20km (measured with the help of scale in ArcGIS software) except for the last straight line, which has a length of 37km. The actual river distance has been measured for every straight line distance, and the SI has been calculated. The straight line has been measured from the upstream to the downstream direction.

6.4 Results

6.4.1 Space and time variability of river temperature

The longitudinal thermal profiles of the entire study stretch have been drawn for the months of February and June of the 5 year period (2014 to 2018) (Figure 6.11). The small stretch of the study area has been shown for the spatial temperature pattern change for the different years. Whatever the season, it seems narrow reaches are warmer than wider ones.

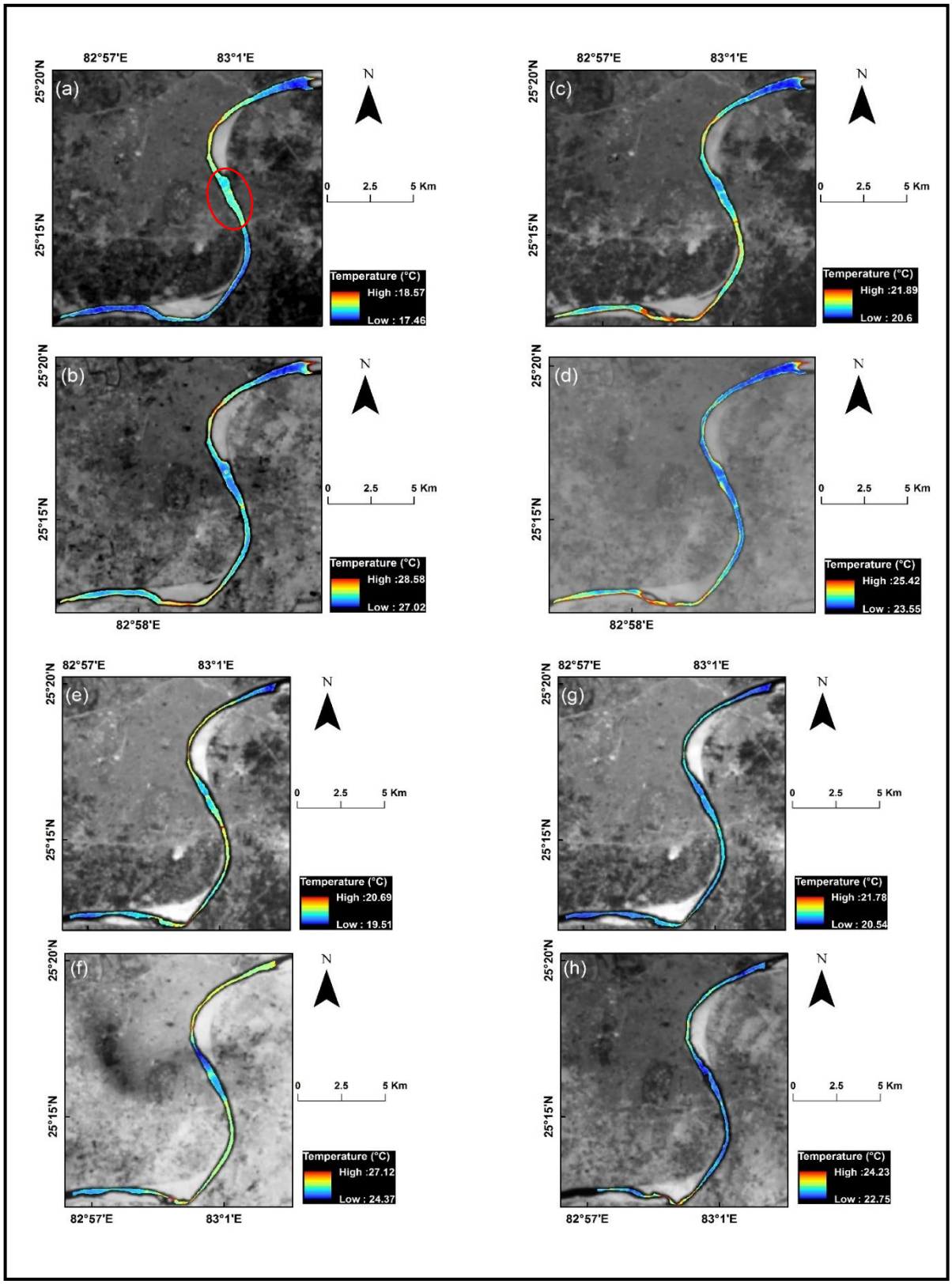

Figure 6.11 (A) Thermal Profile of river Ganga of a sub-reach within the study zone

In figure 6.11 (A), (a) is February 2015, (b) is June 2015, (c) is February 2016, (d) is June 2016, (e) is February 2017, (f) is June 2017, (g) is February 2018, and (h) is May 2018

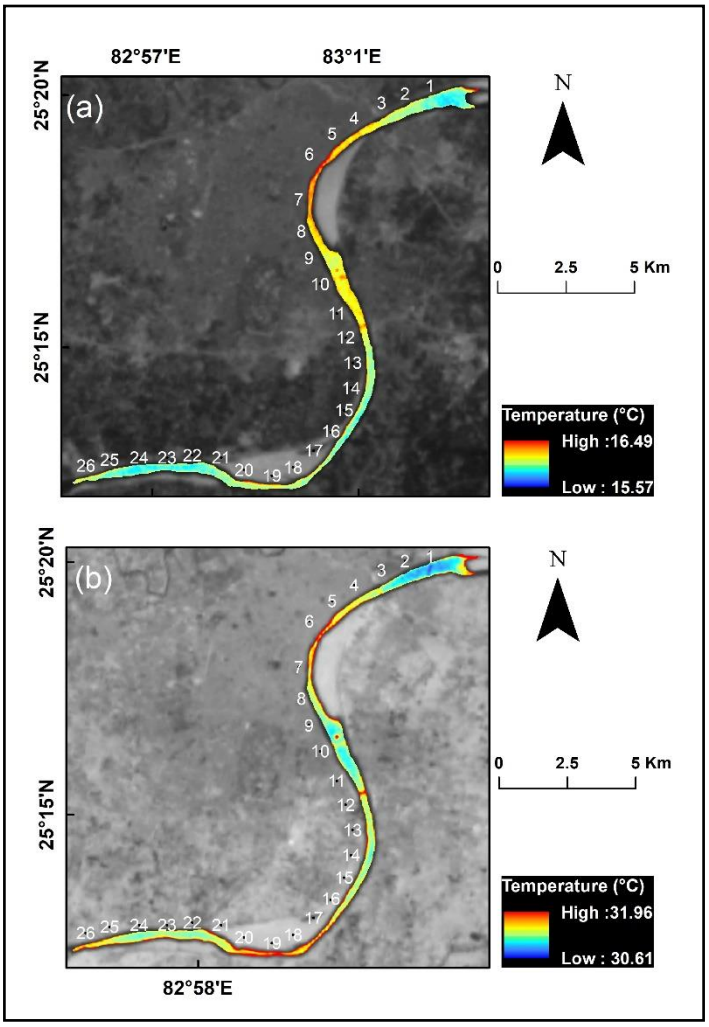

Figure 6.11 (B) (a) is February 2014 and (b) is June 2014

For February 2015 season, the temperature is elevated in the wide region compared to the narrow region. This is due to the presence of the point bar (yellow patches) in the wide region. This phenomenon can be termed as an exception because, for the other seasons, the narrow reaches have more temperature as compared to the wider reaches. The red-oval mark region in (a) depicts this.

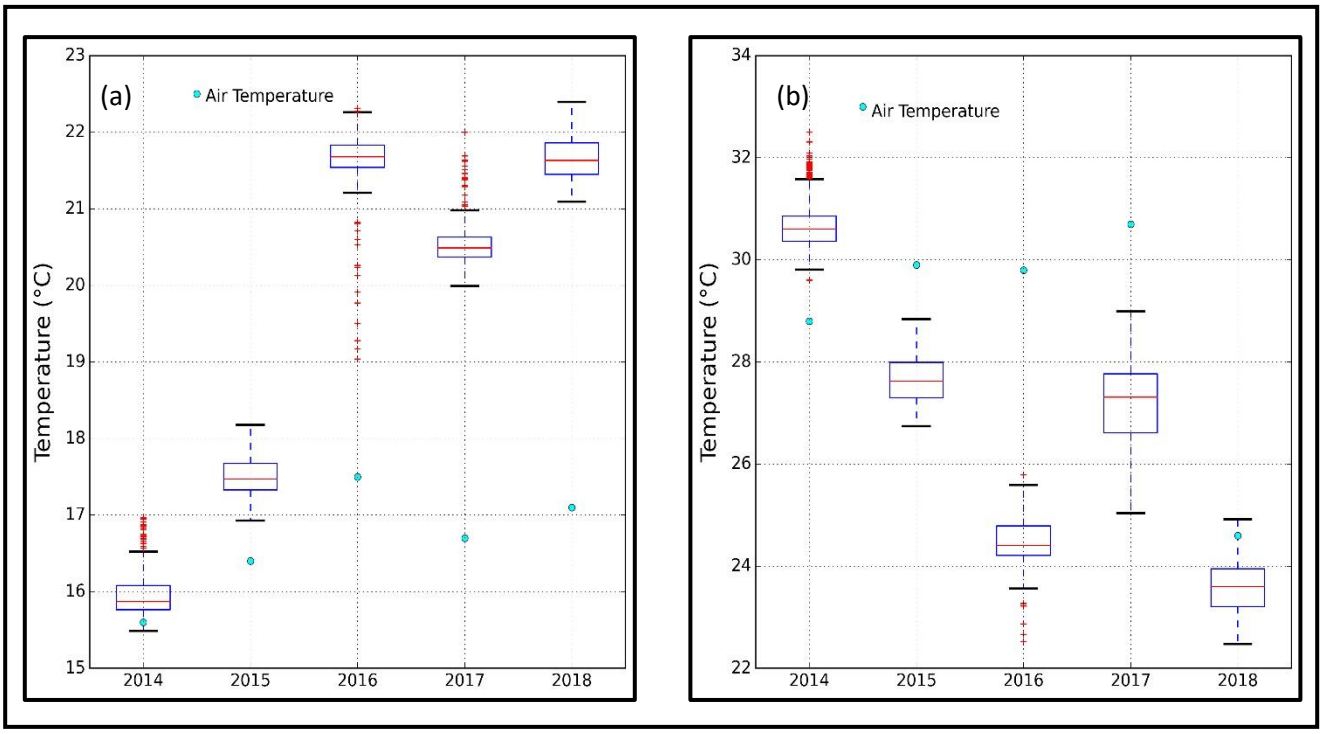

Figure 6.12 Variation of temperature at reach-scale for the different study dates [Horizontal dark lines inside the boxes indicate median values. The width of the boxes indicates the distribution of the temperature corresponding to the interquartile range (Q3(75%)- Q1(25%))]. Graph (a) is for February month and (b) for May 2018 and June months

The temperature for June 2014 shows the highest value for the stretch, and June 2016 depicts the lowest value among the June months. June 2017 shows a higher intra-temperature variation within the considered stretch. The air temperature for the reach for June 2017 has been above 30°C.

For the years 2014 to 2017, there was an increase in median temperature for the month of February and a decrease in river stage values. It has been observed that with the decrease in stage value by 1.18 meters for the month of February between the consecutive years of 2014 and 2015, the median value of the temperature shows a surge of 1.52°C. Similarly, for the years 2015 and 2016, the stage value shows a diminution by 0.61 meters, and there is an

increase in the median temperature value by 4.03°C. The median temperature decreased by 1.09°C for February 2017 in comparison to February 2016, and the stage value increased by 0.29 meters. In 2018 February, there was an increase in stage value by 0.28 meters in contrast to the stage value of February 2017, and the temperature increased by 0.93°C. February 2018 shows a different trend as the stage value increased compared to February 2017 temperature still decreased. In June 2015 stage value increased by 1.05 meters as compared to June 2014, and the temperature value decreased by 2.99°C. In June 2016, the stage value decreased by 0.66 meters as compared to June 2015, and the temperature still decreased by 3.21°C. For June 2017, the stage value increased by 0.34 meters compared to June 2016, but the temperature also increased by 2.9°C. For most of the year under consideration, the month of February shows a trend that when stage value increases, the temperature decreases, and vice versa. Interestingly, June month temperature pattern is not showing the trend of February.

6.4.2 Spatial thermal pattern variation with river geomorphological parameters

Here, all the variations of geomorphological parameters and the temperature have been shown spatially for the entire study stretch. Only three years, namely, 2015, 2016, and 2017 have been considered because the depth values have been available for these three years only. For each of the combined graphs, the first rectangle box has two profiles; one drawn in black is for temperature and another one drawn in red is for depth values. Temperature is measured in ° Celsius, and depth is in meters. The value of the sandbar width is also given in meters. The depth value has not been available for the entire study stretch. The overlapping region of the two satellite scenes has been drawn as a dotted box in figures 6.13, 6.14, 6.15, 6.16, 6.17, and 6.18.

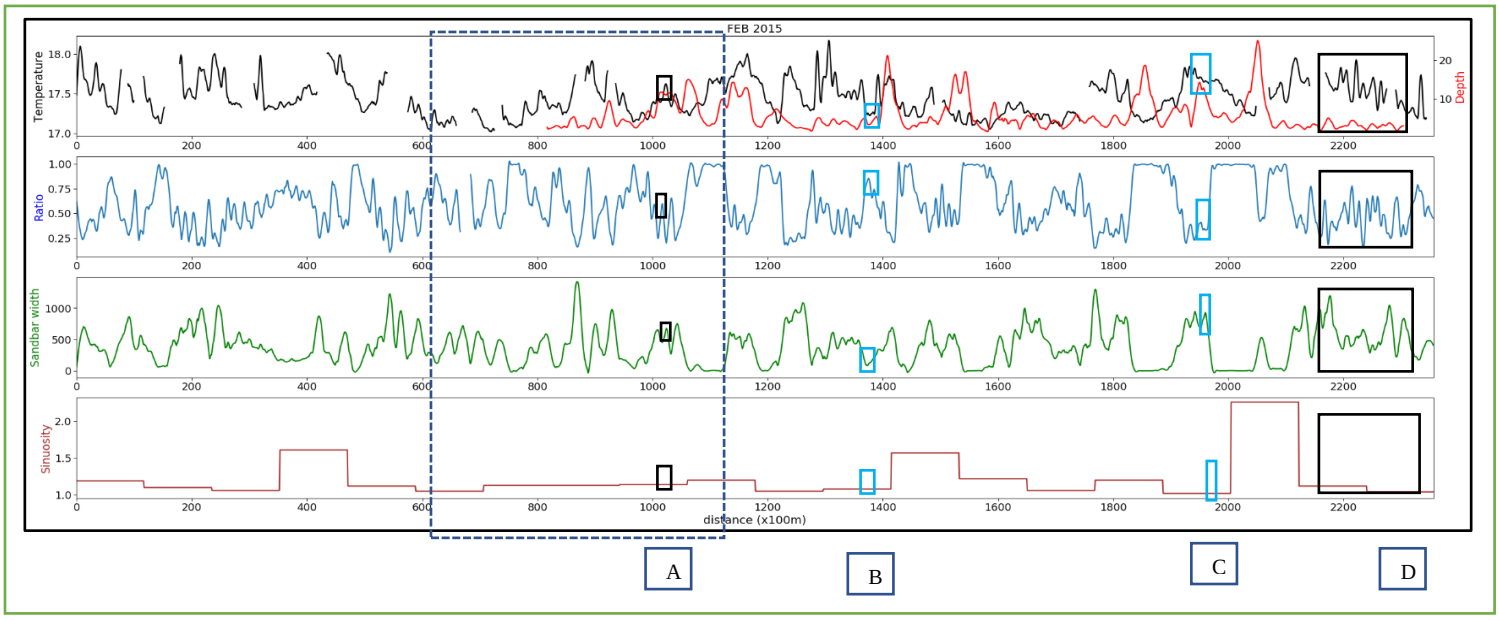

Figure 6.13 Graphical representation of parameters for February 2015

This graph shows the river geomorphological variation during the study stretch for the month of February 2015. From the result, it can be easily observed that as the sandbar width increases by 400meters, and 800 meters, there is a positive change in the temperature by about 0.35°C, and 0.7°C, respectively, and a negative change in the ratio (WW/AW) 0.4 and 0.8. Depth is another factor that affects the temperature of the river. When the depth increases, the temperature decreases. Depth increases by approximately 3meters and 6meters, and the temperature recedes by 0.15°C and 0.3°C approximately. Where the sandbar width is almost constant, there is a minor increase in the temperature of about 0.2°C.

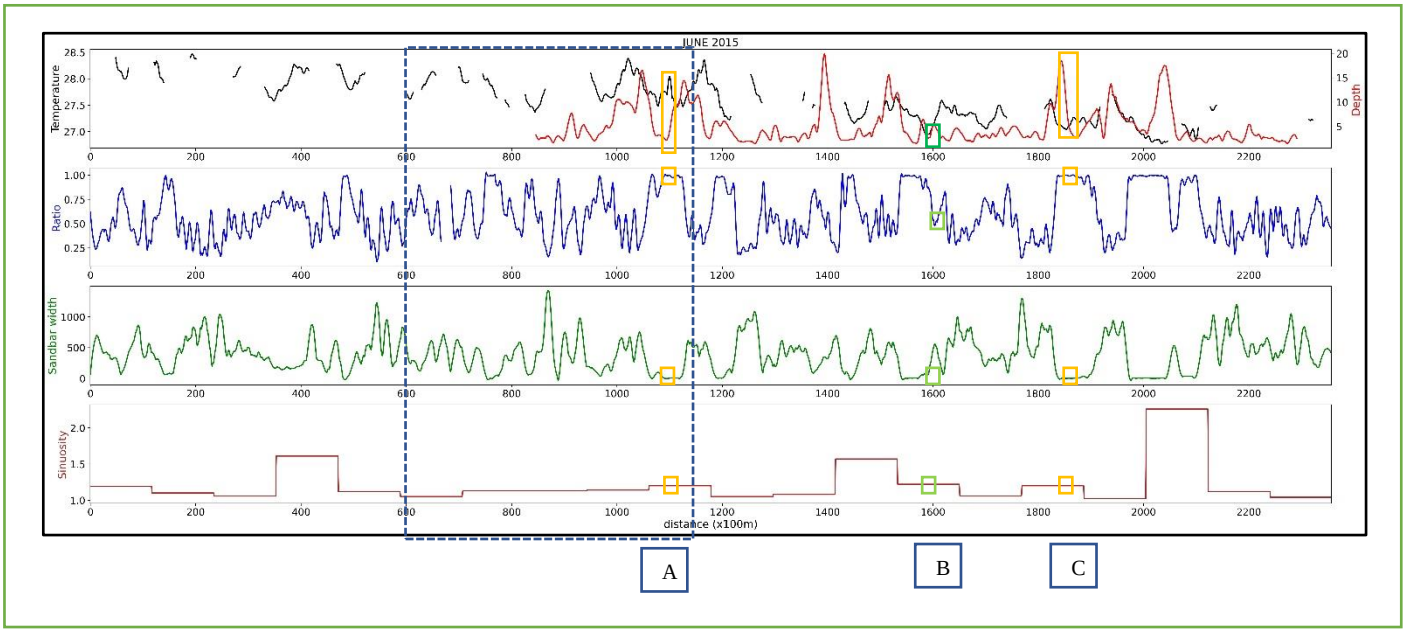

Figure 6.14 Graphical representation of parameters for June 2015

This graph tells the variation of the geomorphological pattern in the study area for June 2015. Results depicted that sandbar width decreases by 900 meters and450meters; then, the temperature value also diminishes by 0.3°C and 0.15°C, respectively. The temperature has a negative relation to the sandbar width. The "ratio" parameter increases by 0.3, 0.6 when sandbar width approximately decreases by approximately 450metrs and 900meters. Depth value also increases by 3 meters, 6meters respectively.

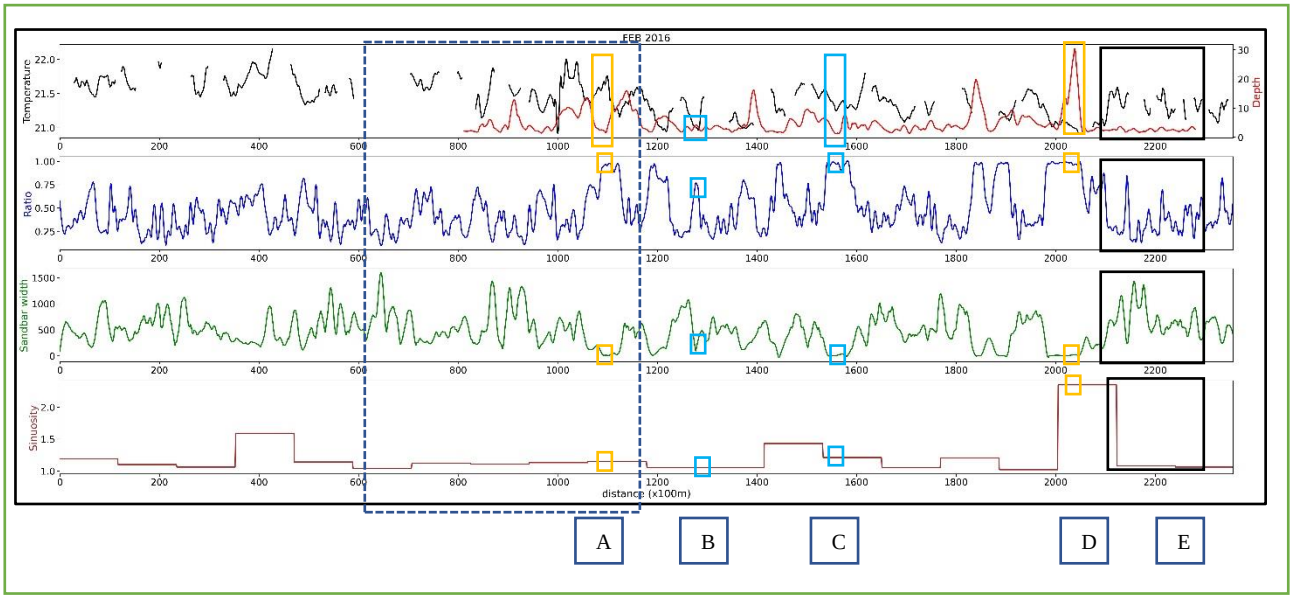

Figure 6.15 Graphical representation of parameters for February 2016

The graph in figure 6.15 is the graph of river geomorphological pattern variation for February 2016 through the entire study stretch. Results show that an increase in sandbars width of about 600 meters, 1200 meters brings the increment to the temperature of the river by 0.25°C, 0.5°C directly, and the ratio changes by 0.5 in inverse proportion. While the depth also affects the temperature of the river. If the depth of the river increases by 4m,12m in a stretch, the temperature of the river decreases by 0.1°C, 0.3°C, respectively. If there is approximately no change in the sandbar width, then depth mostly decreases, and there is no change in the ratio as well.

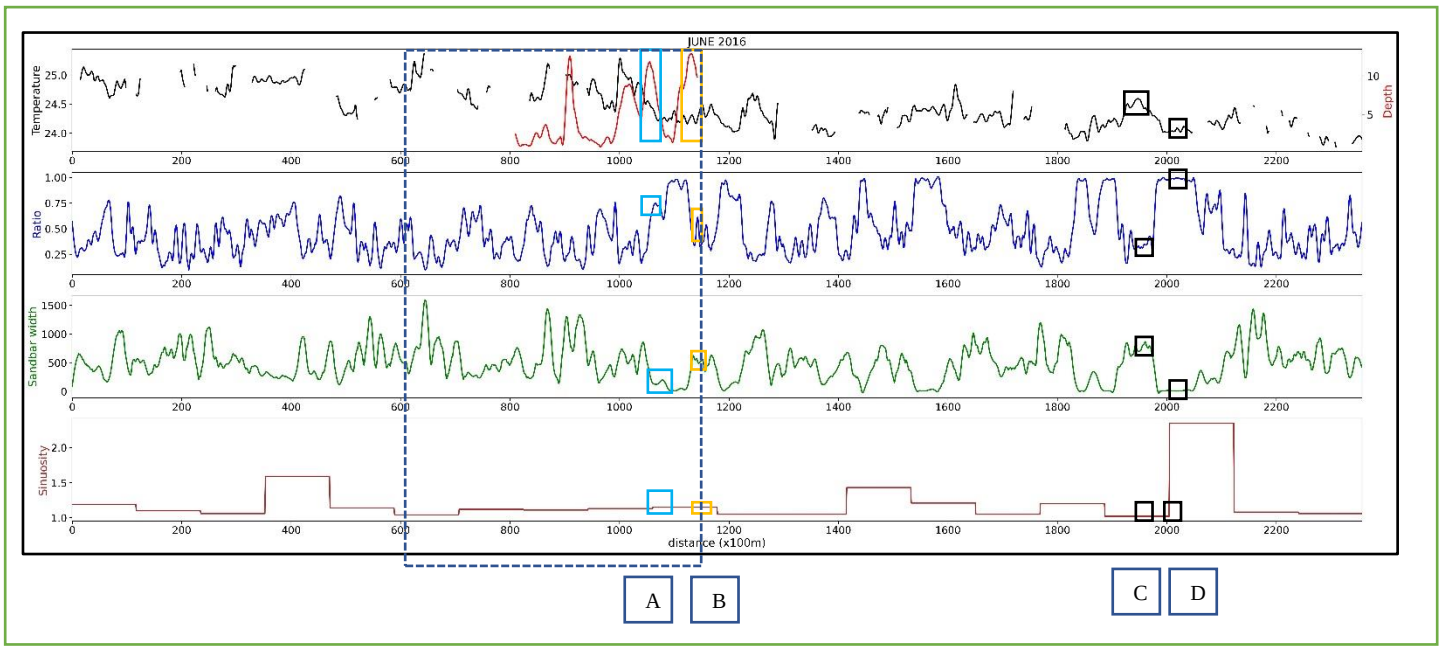

Figure 6.16 Graphical representation of parameters for June 2016

This graph tells the variation of the geomorphological pattern in the study area for June 2016. The graph shows that the ratio parameter shows a decreasing trend when sandbar width increases. The maximum sinuosity region has a sandbar width of less than 500 meters. The sandbar width increases and temperature also shows an increasing trend.

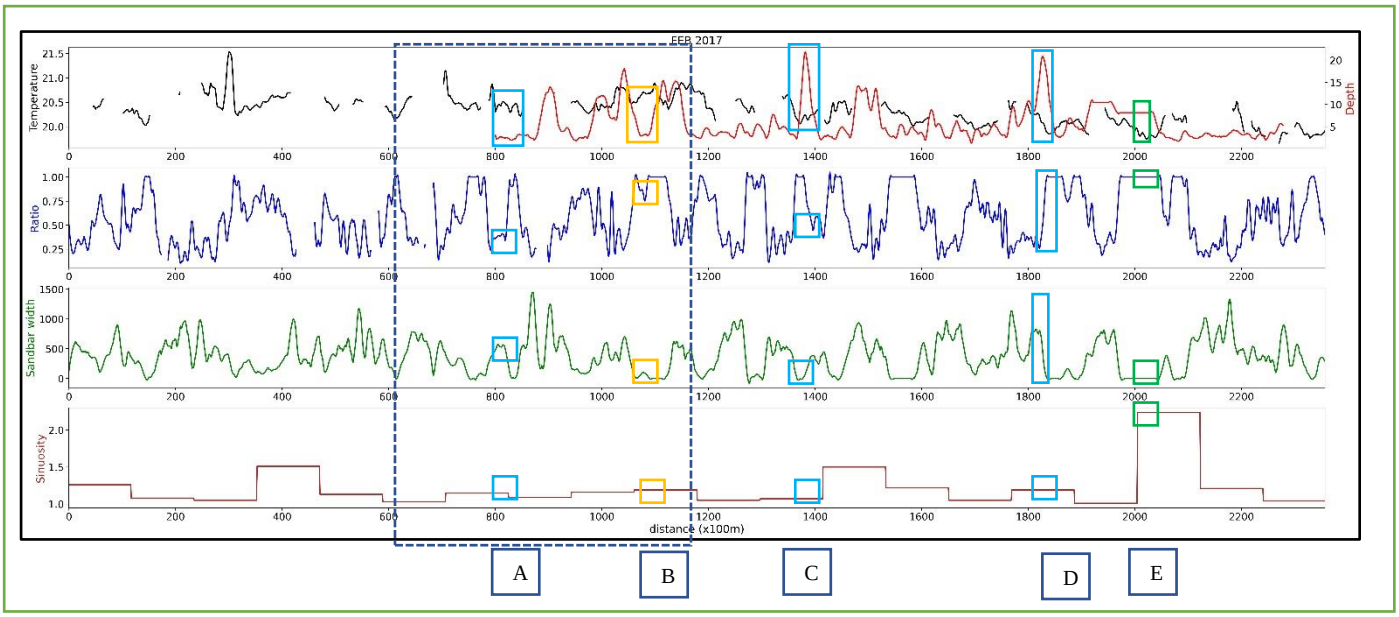

Figure 6.17 Graphical representation of parameters for February 2017

This graph depicts the geomorphological pattern variation for February 2017 in the study stretch.

Results tell that when the "ratio" parameter increases by 0.4,0.8, then the sandbar width decreases by around 500 meters,1000meters, and the temperature also decreases by 0.15°C,0.3°C. River depth also affects the temperature; as depth increases by 2 meters in the stretch, the temperature usually decreases in the range of 0.15°C to 0.2°C and vice versa. When the sandbar width is approximately constant, the temperature usually decreases by 0.1°C, and the ratio remains almost the same.

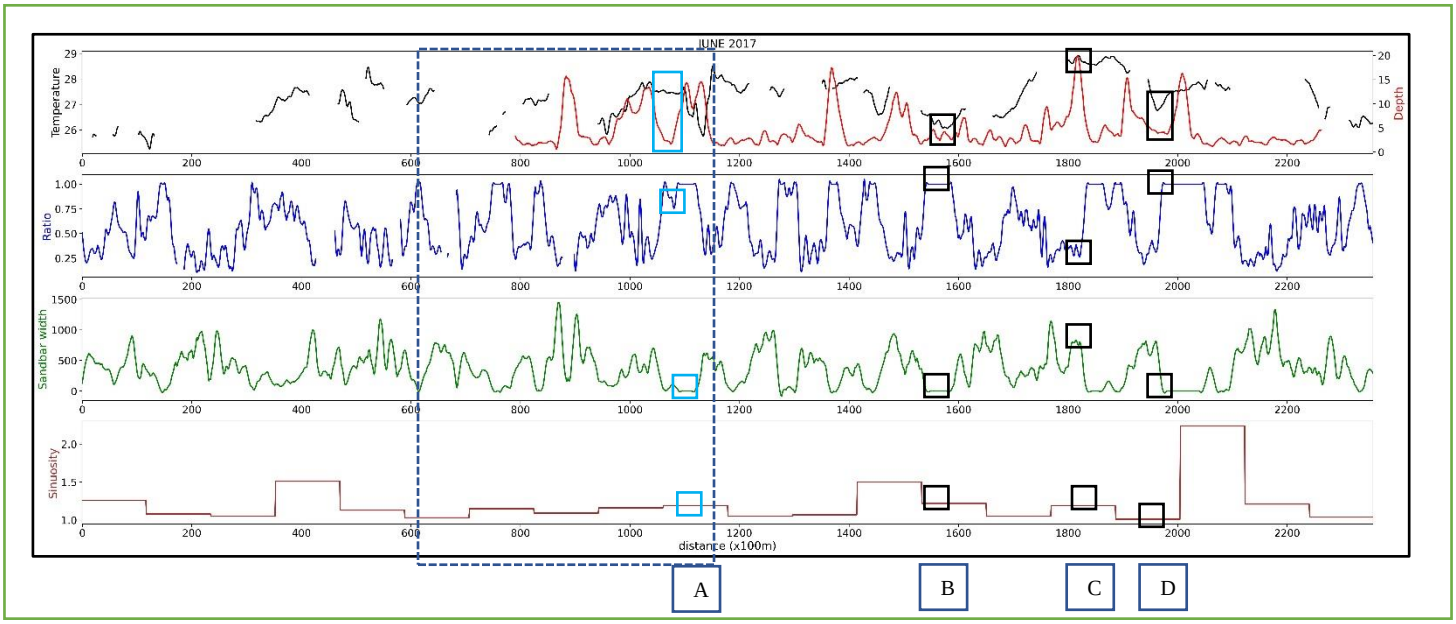

Figure 6.18 Graphical representation of parameters for June 2017

This graph in figure 6.18 tells about the geomorphological variation for the study stretch in June 2017. The result shows that the sandbar width changes by 600 meters, so there is a change of approximately 1°C in inverse proportion. The "Ratio" parameter also decreases by 0.75. The depth parameter also affects the temperature; as the depth increases by about 5 meters the temperature goes down by around 1.3°C. When the sandbar width is almost constant, then there is a slight increase in the temperature by 0.1°C.

6.5 Discussion

6.5.1 Analysis of the river temperature with geomorphological parameters in some specific regions

6.5.1.1 Analysis for February 2015

In region A, the depth varies in direct proportion with that of river temperature. The ratio parameter is comparatively low, and the sandbar width is more than 500 meters. The driving for temperature rise is the sandbar width. In region B, also depth has a direct relationship to temperature. The ratio parameter is high, and the sandbar width is less than 500 meters. Region C shows a similar pattern as that of region A, and that can be seen in figure 6.13**.** There is approximately no variation of depth in region D, but there is enough change in ratio and sandbar width parameter, which influences the river temperature. The depth parameter does not affect temperature regulation in all the regions mentioned above.

6.5.1.2 Analysis for June 2015

The ratio parameter has a value of approximately 1.0, and the sandbar width is almost negligible in region A. The depth value is less than 5 meters, and the temperature value shows an upward spike. Here, depth plays a major role in the temperature rise. In region B, the temperature varies in direct proportion to that of depth. Sandbar width is almost zero, which has an effect on the downward trend of temperature. The sandbar width is the major factor in temperature regulation. In region C, every parameter has its effect on temperature regulation. The low temperature is due to high depth and ratio values as well as negligible sandbar width.

6.5.1.3 Analysis for February 2016

In region A, the depth parameter plays a significant role in the temperature pattern variation of the region. The ratio value is very high, almost 1.0, and sandbar width is almost negligible, but

then also temperature shows an elevating trend. Region B shows the dip in both the temperature and depth value. The sandbar width is also very negligible in this region. The dip in the temperature is caused mainly due to the high value of the ratio parameter. Region C also shows the same trend as region B. All the parameters affect the downward trend of region D. This region has a high depth value along with a very high ratio value of almost 1.0 and negligible sandbar width. There is approximately no variation of depth in region E, but there is enough change in ratio and sandbar width parameter, which influences the river temperature.

6.5.1.4 Analysis for June 2016

All the parameters played their part in regulating the temperature of region A. The high depth value and the ratio value of almost 0.75 and very little sandbar width have propelled the temperature pattern in the downward direction. In region B, depth value plays a major role in the downward fall of the temperature. In this region, the sandbar width is more than 500 meters, and the ratio parameter is also less, but the temperature still has less value. In regions C and D, the depth data have not been available. The temperature in this region is controlled by both the sandbar width and the ratio parameter value.

6.5.1.5 Analysis for February 2017

All the parameters played their part in regulating the temperature of region A. The very low depth value and the ratio value of less than 0.50, and the sandbar width of more than 500 meters have propelled the temperature pattern in the upward direction. In region B, the depth parameter significantly affects regulating the temperature pattern. The ratio parameter and almost negligible sandbar width cannot have that much of an impact on the temperature regulation for this region. In region C, the high depth value and almost nominal sandbar width

are the reason for having low-temperature values. The low ratio value can not elevate the temperature of this region. In region D, the depth value, the ratio value, and the sandbar width all these parameters impact regulating the temperature. The very high depth and high ratio values and decreasing sandbar width make the river temperature in this region relatively colder. In region E, all the parameters have a vital impact on the temperature regulation of this region. The ratio value is almost 1.0, and the sandbar width is virtually negligible in this region.

6.5.1.6 Analysis for June 2017

In region A, the low depth value plays a significant role in the elevated temperature of this region. The ratio value is more than 0.75, and the sandbar width is virtually negligible, but still, they can not bring the temperature down. In region B, the depth and temperature almost follow the same pattern, and low depth can not increase the temperature value. The negligible sandbar width and the high ratio value have more impact on temperature control in this region. In region C, also the depth value does not affect the temperature pattern. The depth value is extremely high, but due to the sandbar width of more than 500 meters and low ratio values, the temperature in this region is high. Region D has a low depth value along with the decline in temperature pattern. The high ratio value and almost negligible sandbar width play a part in this declining temperature pattern of this region.

The sandbar has made the river warmer, and the active channel width also decreases where the sandbars are present. The field sampling has been done in April 2021 also shows the same phenomenon. The sampling has been done for some of the stretches lying inside the study area, and maps are plotted and shown in figures 6.19, 6.20, and 6.21.

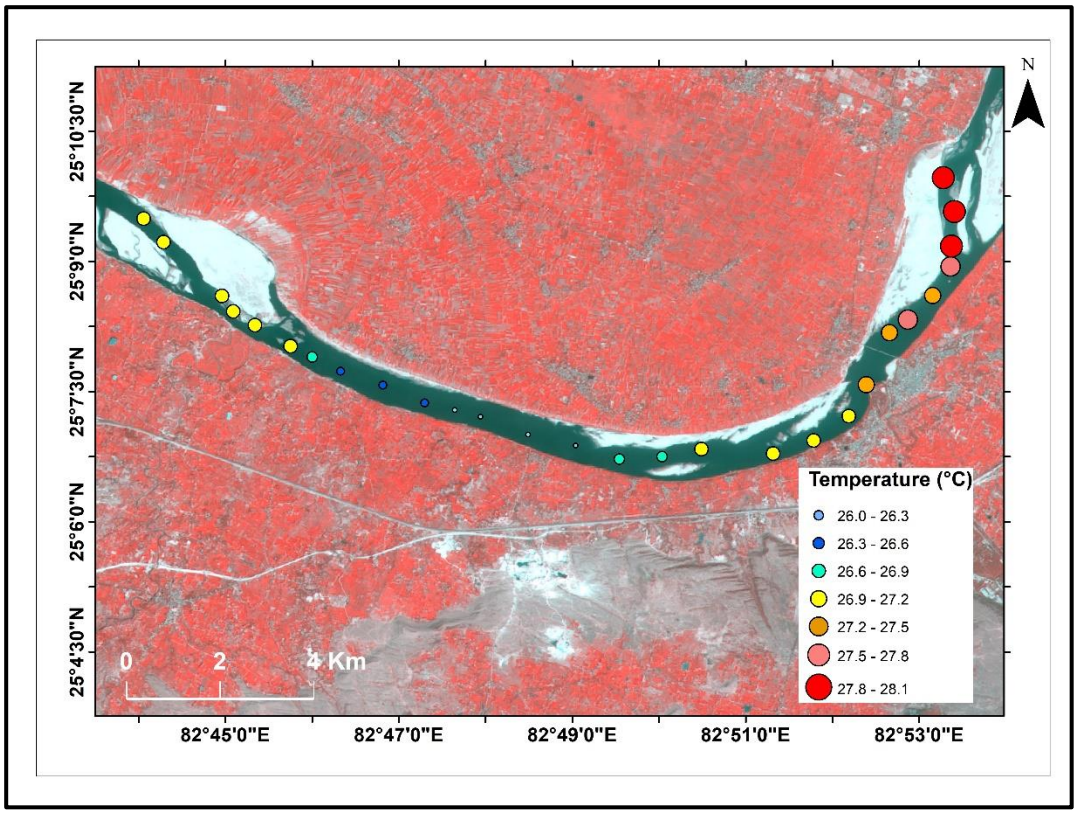

Figure 6.19 Field sampling values for 5th April 2021

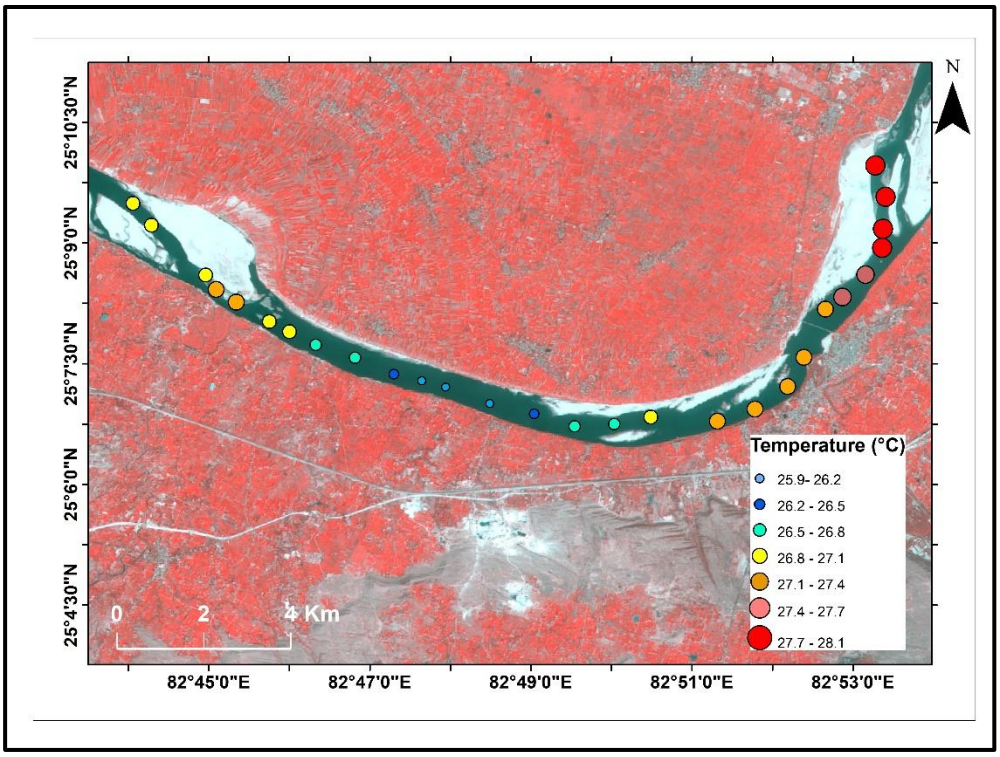

Figure 6.20 Field sampling values for 7th April 2021

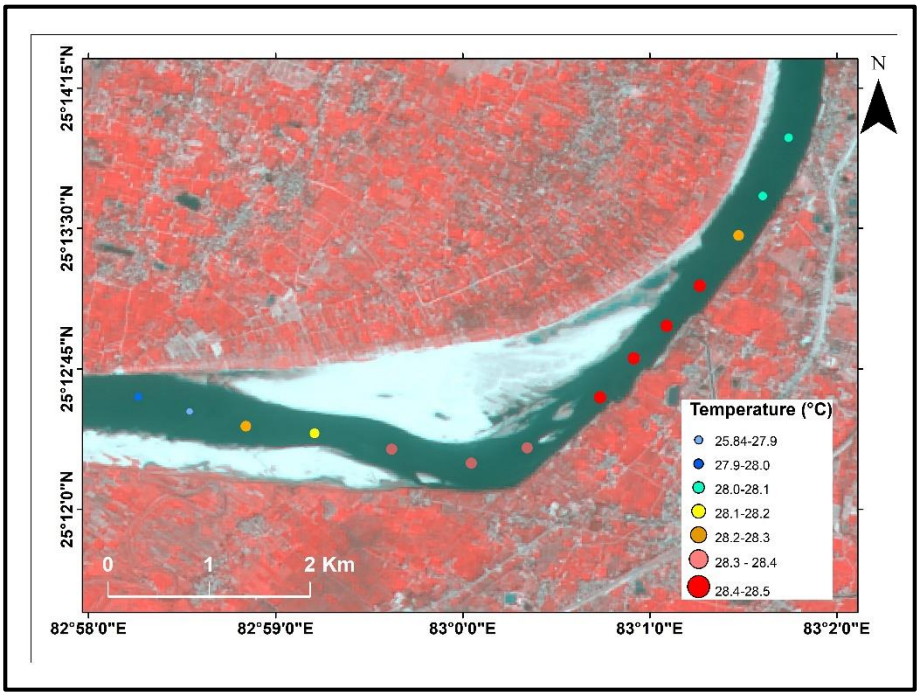

Figure 6.21 Field sampling values for 15th April 2021

Figure 6.22 On-field photographs while doing the in-situ sampling in April 2021

The certain inferences drawn through this intense study may be summarized as follows:

The sandbar has a positive impact on the river's thermal pattern. The WW of the river decreases the river temperature. The regions where the value of WW is more are the places where the river temperature is comparatively cooler than those where WW is less. The depth also has an inverse effect on the thermal pattern of the river. The region of greater depth has mostly lower temperatures compared to the regions with less depth.